CrossMark

ORIGINAL ARTICLE

Cracking and water seepage of Xiashu loess used as landfill cover under wetting–drying cycles

Haijun Lu[1] · Jixiang Li[1] · Weiwei Wang[1] · Changhong Wang[1]

Abstract This paper intends to investigate the anti-seepage characteristics of Xiashu loess used as landfill cover under wetting–drying cycles. A series of tests were performed to systematically evaluate the surface cracks, pores, the hydraulic conductivity and water seepage of the soil under wetting–drying cycles. The cracking tests indicated that the cracking intensity factor (CIF) increased with the number of wetting–drying cycles. After three wetting–drying cycles, the CIF gradually reached a stable value. The influence of the compactness of the compacted clay was significant to cracking. After four drying–wetting cycles, the CIF of compacted clay with relatively low compactness ($\rho = 1.65$ g/cm^3, $W_5 = 25$ %) was 0.15, and the CIF of compacted clay with higher compactness ($\rho = 1.65$ g/cm^3, $W_3 = 21$ %) was only 0.06. With the increase in the number of wetting–drying cycles, the accumulated pore volume of the soil particles increased and the maximum pore size was nearly unchanged. After four drying–wetting cycles, the proportion and average diameter of macro-pore in the soil particles were both increased. However, the proportion and average diameter of the meso-pore slightly decreased. Furthermore, the proportion and average diameter of the micro-pores were unchanged. After four wetting–drying cycles, the hydraulic conductivity of the compacted soil was at 8.3×10^{-7}–1.5×10^{-5} cm/s, which was increased about three orders of magnitude compared with the compacted soil without cracks. The hydraulic conductivity of compacted soil increased linearly as cracks increased. The hydraulic conductivity of compacted soil also gradually increased to a stable value as the pore volume increased. After 1 month of wetting–drying cycles, the cracks of soil with low compactness had extended to a depth of 15 cm below the soil surface while the cracks of soil with higher compactness only reached a depth of 5 cm.

Introduction

When the storage limit of a landfill is reached, a cover system is constructed to reduce the leachates from the municipal solid waste (MSW) and protect the ecological environment. A typical landfill cover system consists of a vegetation layer, a drainage layer and an impervious layer. According to the "Technical code for municipal solid waste sanitary landfill (CJJ 17 2004)", compacted clays are often used to construct the impervious layer with a hydraulic conductivity of less than 1×10^{-7} cm/s. Enormous heat is generated during the degradation process of household refuse in the landfill, which leads to an increase in temperature in the landfill. On the one hand, the differences in temperature between the outside and inside of the landfill result in the moisture transferring in the form of vapor from high temperature to low temperature zones. On the other hand, liquid water flows from low temperature to high temperature zones under the influence of the matric potential (Döll 1997; Zhou and Rowe 2003). This above-mentioned water transport would result in a continuous decrease in the moisture content in the landfill cover. It is well known that compacted clays often subject to desiccation crack during drying (Tang et al. 2008, 2010; Li and

✉ Jixiang Li
jixiang_li@163.com

[1] Institute of Poromechanics, Wuhan Polytechnic University, Wuhan 430023, China

Zhang 2011; Li et al. 2011). Consequently, the landfill cover, which is made of compacted clay, cracks due to desiccation shrinkage (Hewitt and Philip 1999; Lecocq and Vandewalle 2003; Basnett and Bruner 1993). Once cracked, rainfall can easily infiltrate into the landfill cover and lead to an increase in leachate from the MSW in landfill. The wetting–drying cycles have significant influence on the cracking of the compacted clay. With the accumulation of wetting–drying cycles, the cracking of compacted clay becomes more and more severe (Yesiller et al. 2000; Rayhani et al. 2008).

Once a crack forms in the landfill cover, the hydraulic conductivity of the clay significantly increases. In the meantime, the landfill cover system loses its anti-seepage function. Albrecht and Benson (2001) reported that the hydraulic conductivity of cracked clay became 1000 times larger than that of an intact soil. Desiccation cracks can further develop under the wetting–drying cycles. On the one hand, when the desiccation cracks penetrate through the compacted clay landfill cover system, the hydraulic conductivity of the compacted clay is dominated by cracks. On the other hand, clayey soils swell during wetting, which can partially heal the crack. Under this condition, the hydraulic conductivity is controlled by both cracks and the micro-pores in the clay. The wetting–drying cycles have significant influence in the soil structure as well as the loss of cohesion between soil particles. Therefore, the soil structure is shattered, resulting in increases in both the pore size and the number of pores in the clay.

Xiashu loess is widely distributed loessal sediment in the middle and lower reaches of Yangtze River in China. This paper systematically investigated the development of cracks in the loess used as landfill cover and the associated changes in soil permeability under wetting–drying cycles. The mechanisms of surface cracking the loess were studied using a cracking monitoring device with four wetting–drying cycles. The transformations of pore structure of the loess were analyzed using the low temperature N_2 adsorption tests. The hydraulic conductivities of cracked loess were determined using the PN3230M environmental soil flexible wall permeameter. The rainfall infiltrations were measured by a seepage-monitoring device for the cracked loess.

Materials and methods

Testing materials

The loess of 500 kg was obtained from a construction site named as Jinyintang subway station in Changqing Garden, Wuhan City, Hubei Province, China. Firstly, the obtained soils were air-dried, and the clods were carefully crushed with a rubber mallet to avoid breaking the grains. The crushed soils were passed through a 2 mm sieve to eliminate the large particles. The physical properties, the chemical properties and the mineral compositions of the soil are given in Tables 1 and 2, respectively. The SEM micrograph of the soil is shown in Fig. 1.

Test methods

Soils were compacted at a given target dry density (1.65 g/cm^3) with different initial moisture contents (17, 19, 21, 23, 25 %). Soil specimens were then cut from the compacted soil samples using cutting rings. The obtained soil specimens, together with the cutting rings, were subjected to 4 cycles of alternate wetting and drying in the laboratory. The specimens were first dried at 40 °C. Complete drying of the specimens took about 5 days. The dried specimens were then put on the porous stone and wetted by absorbing moisture from a wet sand bath at the bottom for about 1 day. Following near saturation, the specimens were again dried at 40 °C. During the drying–wetting cycles, the weight of the soil specimen was measured by using an electronic balance from which the moisture contents were determined. The surface cracks of compacted soil samples were monitored by using a digital microscope camera with a magnification ratio of 10 times (Fig. 2).

A JW-BK static nitrogen adsorption instrument (Beijing JWGB Sci. & Tech. Co., Ltd.) was used to measure the pore structure of soil specimens. The instrument measured the static adsorption isotherms under the saturation temperature of liquid nitrogen. The relative pressure was within 0–0.99. A total of 22 specific pressure spots was taken for the isothermal absorption, and 22 specific pressure spots were taken for the isothermal desorption to detect the specific area, pore diameter, and pore-volume distribution of soil specimens (Xue et al. 2014a).

The PN3230M environmental soil flexible wall permeameter, manufactured by GEOEQUIP, Inc., was used to measure permeabilities of the soil specimens under different wetting–drying cycles. The permeameter can prevent the sidewall leakage caused by the specimen's volume change during the wetting–drying cycles. The specimens used in the permeability tests have dimensions of 5 cm in diameter and 5 cm in height. All samples were made by statically compacting soil of specific quantity into a model with the above-mentioned dimension. The samples were then submerged in water and vacuum was applied for 1 day to saturate the soils before the permeability tests. After that, the soil specimens were placed in an oven at 40 °C for 5 days after permeability tests. This constituted one wetting–drying cycle and the process was repeated for four times.

Table 1 The physical properties of the loess

Maximum dry density (ρ_{dmax}) (g/cm³)	Optimum water content (W_{opt}) (%)	Liquid limit (W_L) (%)	Plastic limit (W_P) (%)	Plasticity index (I_p) (%)	Porosity ratio (e)	Specific gravity (G_s)	Hydraulic conductivities (K_s) (cm/s)	Particle size distribution (%)			
								>0.05 mm	0.05–0.005 mm	0.005–0.002 mm	<0.002 mm
1.65	19	48.5	26.2	22.3	1.4	2.68	2.5×10^{-8}	12	32	45	11

A water seepage test was conducted for the compacted soils during the action of four wetting–drying cycles. As shown in Fig. 3, the inner diameter and the height of the container are 50 and 20 cm, respectively. The soil samples used have dry unit weight of 1.65 g/cm³ and moisture content from 21 to 25 %. The wetting–drying cycles were simulated using a heating source and a rainfall simulator which lasted for 29 days. A 3 cm thick rubber blanket was installed along the inner-wall of the container to prevent the possible water flow along the container wall. The moisture sensors were installed at 5, 10, and 15 cm depths below the surface of soil layer to monitor soil moisture contents at different times. The rainfall intensity used was 20 mm/day to evaluate the percolation behavior of the cracked clay. The 1 day-long rainfall was conducted by a rainfall simulator.

Results and discussion

Cracks

The surface cracks of the compacted soil after four wetting–drying cycles are shown in Fig. 4. After four wetting–drying cycles, cracks were observed on all specimens. The most significant cracking appeared on those specimens with dry density of 1.65 g/cm³ and the initial moisture content of 25 %. The cracks were crisscrossed and the soil particles were badly shattered around the cracks. The samples with initial moisture content of 21 % had relative less cracks on its surface. This happened because that a lot of water in the soil was lost after the desiccation. The effective lateral confining stress of soil particles became smaller than the pore water pressure, resulting in the cracking of the loess. The drying shrinkage of a compacted soil would lead to irreversible changes in soil structure, which include loss of bonding between soil particles and reduction in strength.

The cracking intensity factor (CIF), which is the ratio of cracked area to the total area (Miller et al. 1998; Yesiller et al. 2000), was used to characterize the surface cracking of compacted soil samples. The color of the un-cracked area was brighter than that of the cracked area. The differences in color can be used to calculate the CIF through a digital microscopic image analysis software.

The crack development of the soil samples under the action of the wetting–drying cycles is shown in Figs. 5 and 6. It can be seen that the CIF of the soil samples gradually increased with the decrease in the moisture content, indicating that the continuous loss of water in the soil induced the crack growth. During the wetting–drying cycles, the CIF of the soil samples firstly decreased with the increase of the moisture content, and then gradually

Table 2 The chemical properties and the mine components of the loess

pH	Soluble salt (%)	Organic matter (%)	Mine components (%)				
			Chlorite	Kaolinite	Illite	Quartz	Feldspar
5.8	0.5	1.2	22	15	24	34	5
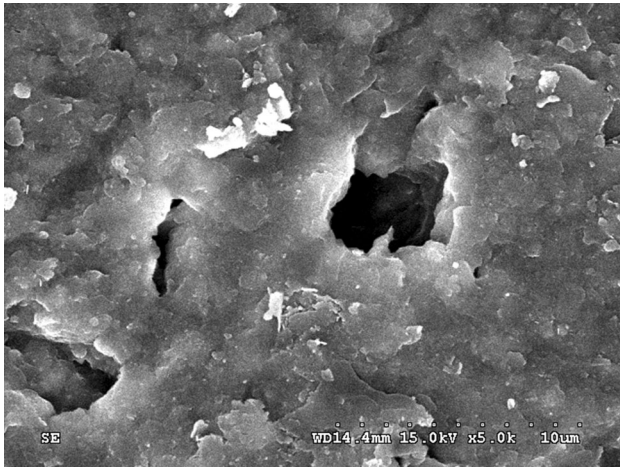
Fig. 1 The SEM micrograph of the loess
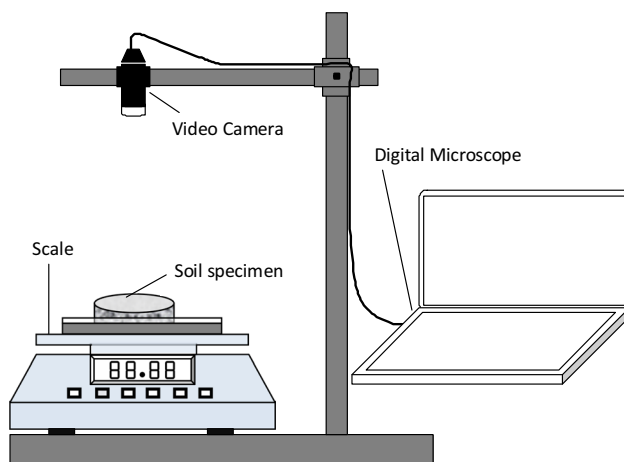
Fig. 2 Cracking monitoring device of compacted soils

increased with the continuous drying, which suggested that at the beginning of the wetting process, because of the swelling of soil particles, part of the cracks on the soil surface closed even disappeared. In the following drying process, the healed cracks cracked again and the cracking was much more severe than before. In the wetting process, the adhesiveness between soil particles was weakened, resulting in the shattering of the particles. The phenomenon was more significant on the surface layer. During drying, the soil shrank, resulting in the cracking on the weakest part in the soil samples. Quartz and feldspar is non-swelling mineral. Illite itself is a non-expansive

mineral. However, when it reacts with weakly acidic water, K^+ ion will be leached out, substituted by other ions such as Na^+, Ca^{2+} or H_2O and result in swelling. Chlorite is normally non-expansive, but degraded chlorite will swell in a way similar to the illite when it loses K^+ ions. Kaolinite, acidified illite and degraded chlorite has the expansibility. Hence, a complex cracking (opening/closing of cracks) is characteristic for the loess (Montes-H et al. 2003; Montes et al. 2004).

The wetting–drying cycles had significant influence on the cracking of compacted soils. The CIF of compacted soils rapidly increased with the increase in the numbers of wetting–drying cycles. However, after three wetting–drying cycles, the increase in CIF apparently slowed down and then gradually reached a stable value. After four wetting–drying cycles, the CIF of the compacted soil samples was 0.15, 0.14, 0.13, 0.09, and 0.06 for moisture contents of 25, 17, 23, 19, and 21 %, respectively.

Pores

The adsorption and desorption isotherm of the compacted soil samples is shown in Fig. 7. The distributions of pore volume and pore size are shown in Fig. 8. According to the IUPAC classification method, the adsorption isotherm of soil belongs to the typical II which was only reversible on the multilayer of macro-solid. The adsorption isotherm did not completely coincide with the desorption isotherm and the type H_3 hysteresis loop appeared on the curve, indicating that the pore size distribution of soil was widespread. The hysteresis loop was relatively large and the regenerated pores in the loess were dominant. According to the IUPAC classification method, micro-pore is smaller than 2 nm, macro-pore is larger than 50 nm, and the meso-pore is between 2 and 50 nm. In the soil tested, there were less micro-pores and more meso-pores which spread widely, and the pore size peaked at 3.2 nm. The pore volume increments of soil peaked at 7.9 nm with the accumulated pore volume of 0.36 cm^3/g. It can also be seen that the accumulated pore volume rapidly increased at the peak of increment pore volume.

The changes of pore volume and pore size distributions in the wetting–drying cycles are shown in Figs. 9 and 10. The curve of pore size had a peak with relatively wide shoulders, and the proportion of pore between 2 and 7 nm was relatively large. The curve of the accumulated pore volume was close to straight line. The distribution of the

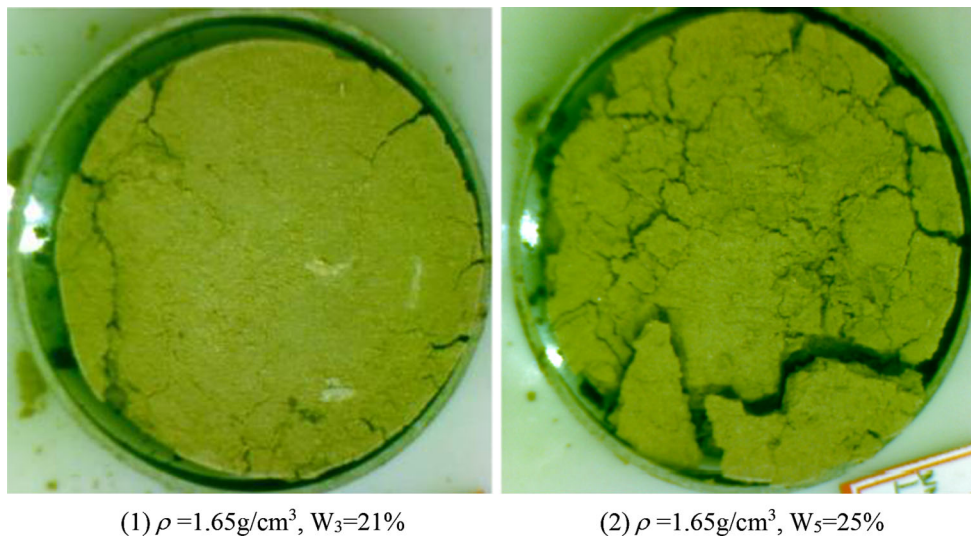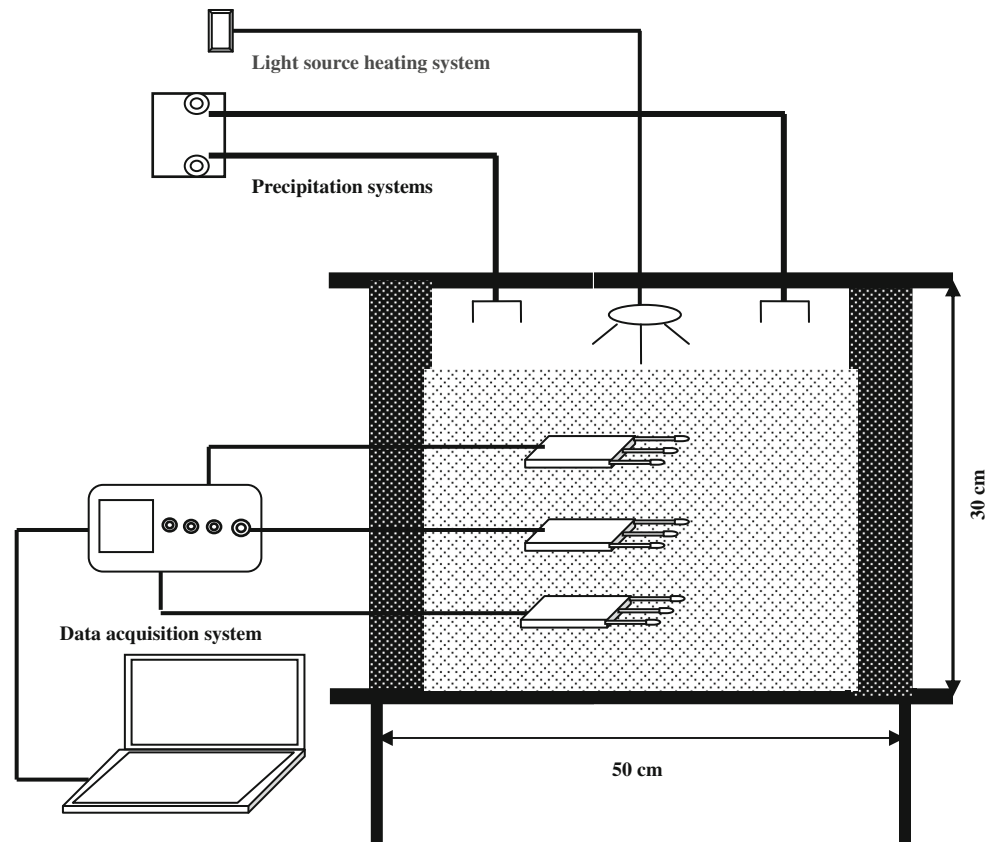**Fig. 3** Water seepage testing device for cracked soils

Fig. 4 The surface cracks of the compacted loess after four wetting–drying cycles

(1) ρ =1.65g/cm^3, W_3=21%   (2) ρ =1.65g/cm^3, W_5=25%

pore volume was uniform. For the specimen ($\rho = 1.65$ g/cm^3 and $W_5 = 25$ %), the accumulated pore volume after the first wetting–drying cycle was 0.378 cm^3/g. With the increase in the number of wetting–drying cycles, the accumulated pore volume continuously increased. After four wetting–drying cycles, the accumulated pore volume reached 0.513 cm^3/g. However, the maximum value of pore size had hardly changed in the four cycles. After the wetting–drying cycles, the average diameter and proportion of macro-pore were both increased. The average diameter and the proportion of meso-pore slightly decreased and that of the micro-pore kept unchanged.

(1) ρ =1.65g/cm^3, W$_3$=21%
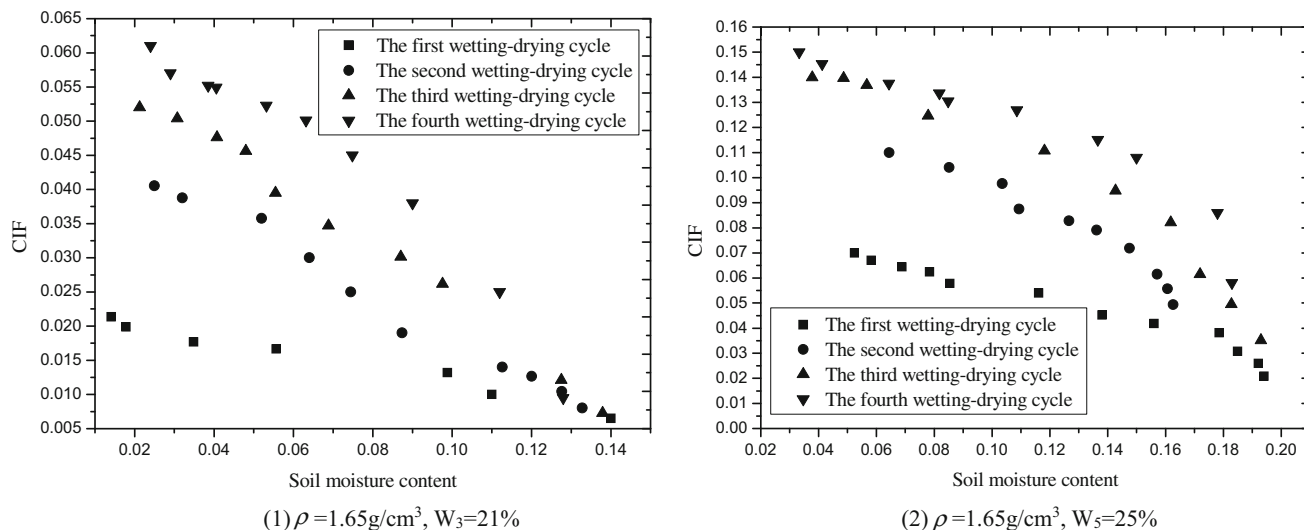

(2) ρ =1.65g/cm^3, W$_5$=25%

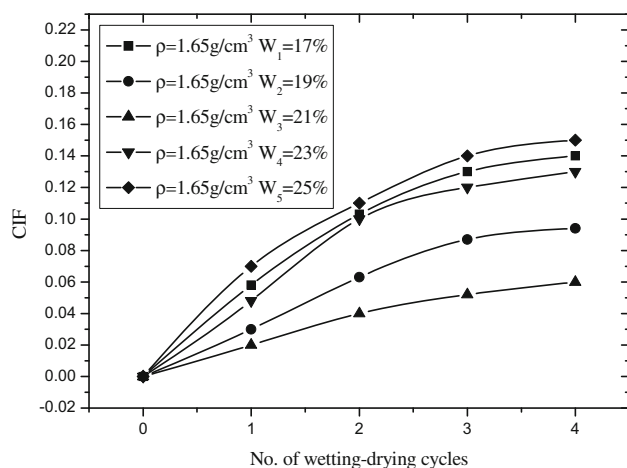Fig. 5 The CIF of compacted loess during wetting–drying cycles

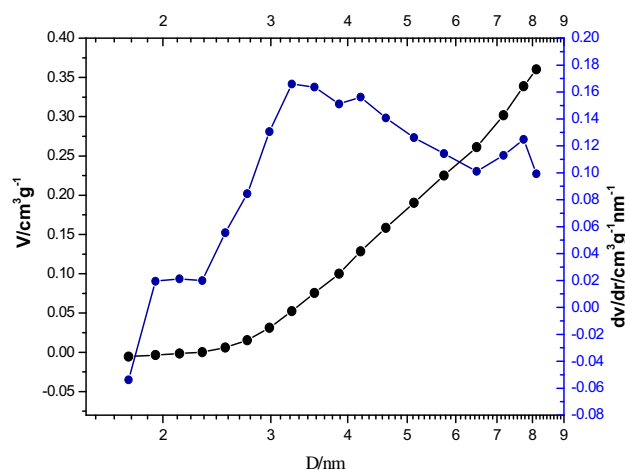Fig. 6 The relationship between the CIF and number of wetting–drying cycles

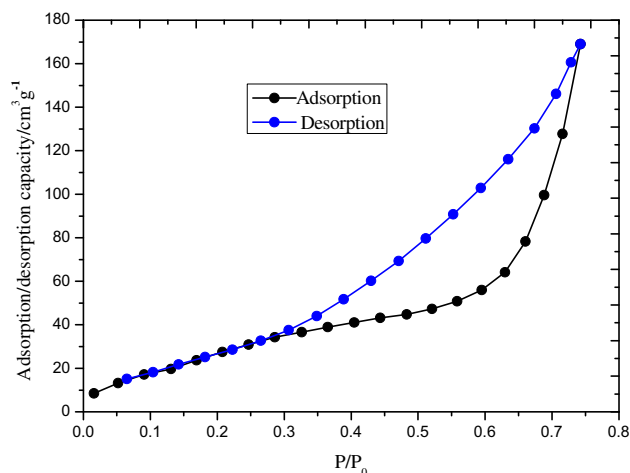Fig. 8 The distribution of pore volume and pore size of the loess

In the wetting process, with the water penetrating into the loess, the absorbed water between soil particles became thicker, and the soil skeleton structure swelled. Meanwhile, there are the relative movements between soil particles due to chemical dissolutions. Thus, a new stable structure gradually formed based on the old broken structure.

In the drying process, the moisture content of soil gradually decreased, and the shrinkage of soil destroyed the soil structure again. On the one hand, part of the meso-pore and micro-pore was transformed to macro-pore because of chemical dissolutions. On the other hand, part of micro-pores expanded and enlarged because of the drying shrinkage which helped increase the amount of meso-pore and macro-pore in the soil, and enlarged the pore volume. Under the action of wetting–drying cycles, the structure of soil was destroyed time by time. The strength of soil was
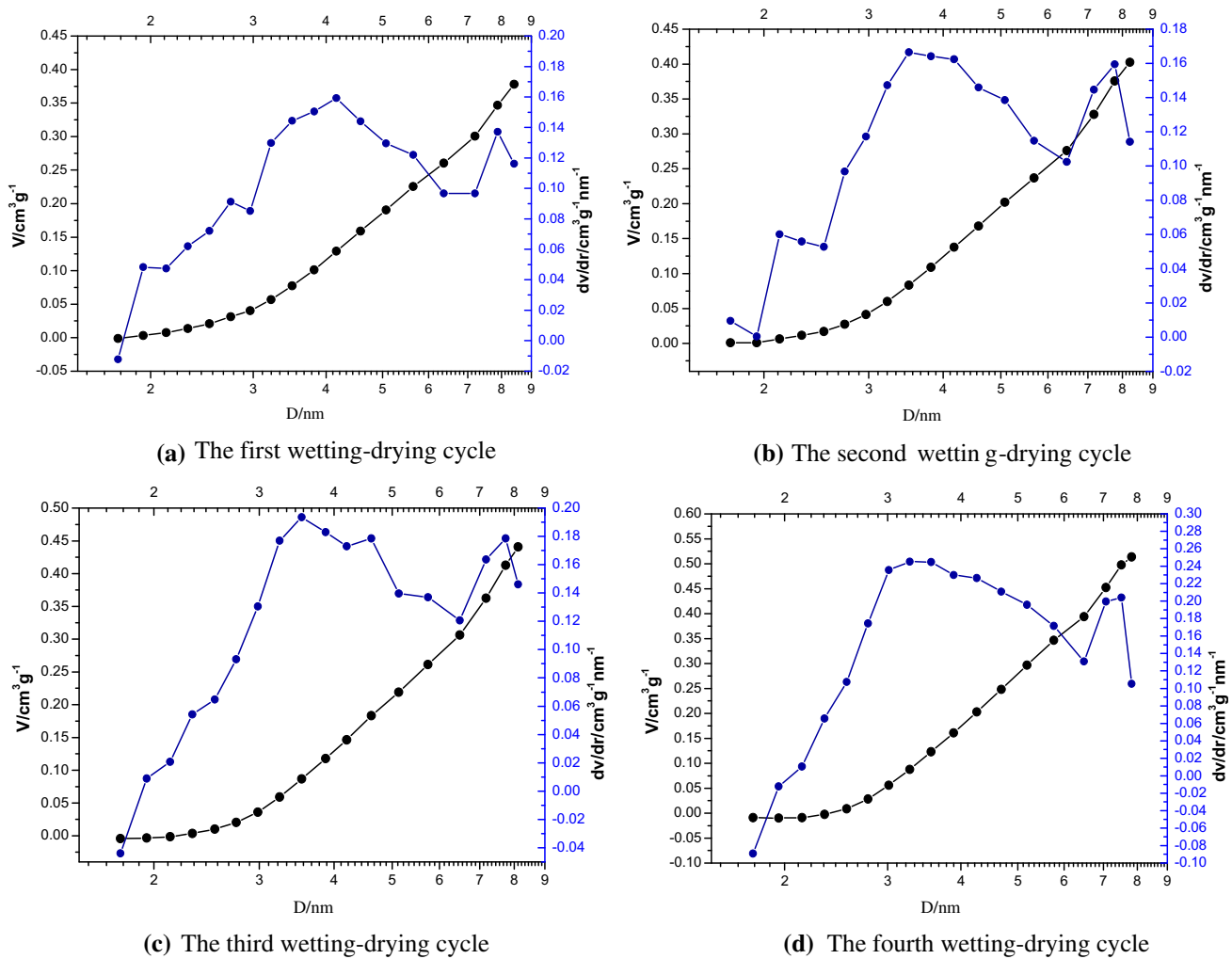

Fig. 7 The adsorption and desorption isotherm of the loess

(a) The first wetting-drying cycle

(b) The second wetting-drying cycle

(c) The third wetting-drying cycle

(d) The fourth wetting-drying cycle

Fig. 9 The distribution of pore volume and pore size of the loess during wetting–drying cycles. ($p = 1.65$ g/cm^3, W5 = 25 %)
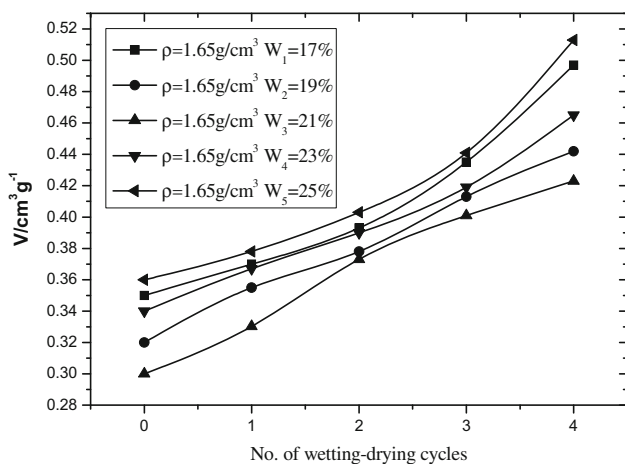

Fig. 10 The pore volume of the loess during wetting–drying cycles

weakened. But with increase in wetting–drying cycles, the soil structure would be gradually stabilized.

Hydraulic conductivity

The hydraulic conductivity of the soil specimens during the wetting–drying cycles is shown in Fig. 11. The relationship between the hydraulic conductivity and the cracks, and pores of compacted soil is presented in Figs. 12 and 13, respectively. The wetting–drying cycles have significant influences on the hydraulic conductivity. Specifically, the hydraulic conductivity of soil rapidly increased with the accumulated number of wetting–drying cycles. The trend was more obvious in the first two cycles. At the end of the third wetting–drying cycle, the increase in the hydraulic conductivity slowed down apparently and then gradually stabilized. As for
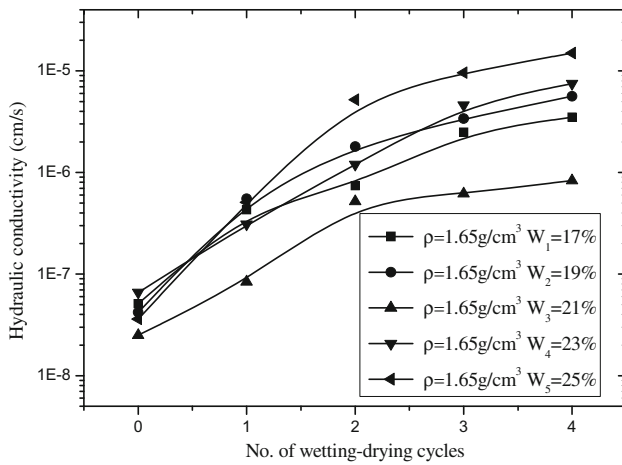
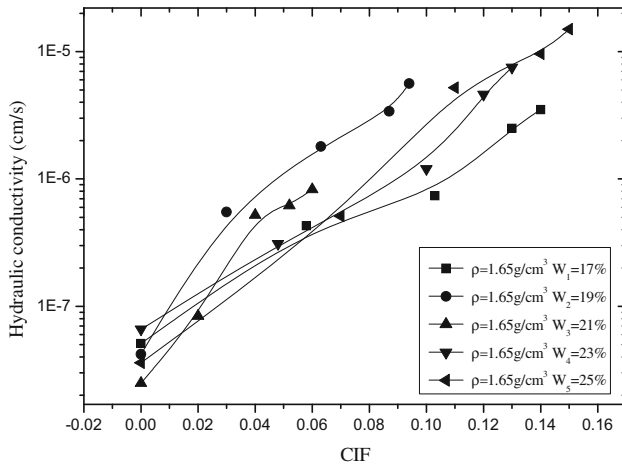Fig. 11 The hydraulic conductivity of the loess during wetting–drying cycles

Fig. 12 The relationship between the hydraulic conductivity and the cracks of compacted loess
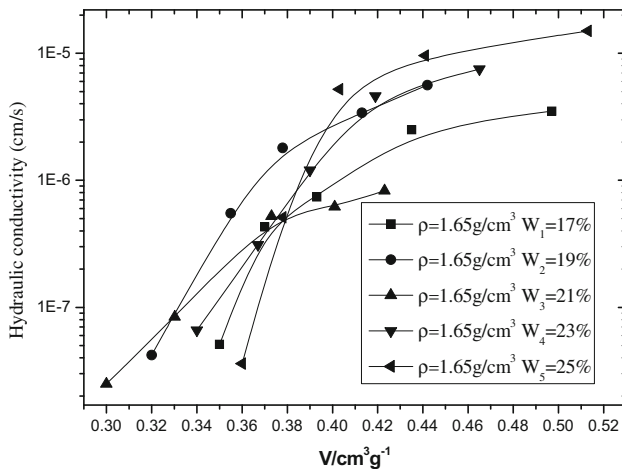

Fig. 13 The relationship between the hydraulic conductivity and pore volume of compacted loess

the badly cracked soil specimen ($\rho = 1.65$ g/cm^3, $W_5 = 25$ %), after four wetting–drying cycles, the hydraulic conductivity rapidly increased about three orders of magnitude (from 3.6×10^{-8} to 1.5×10^{-5} cm/s). In addition, hydraulic conductivity of the specimen ($\rho = 1.65$ g/cm^3, $W_3 = 21$ %) increased about one order of magnitude (from 2.5×10^{-8} to 8.3×10^{-7} cm/s). It was larger than the value of 1×10^{-7} cm/s, indicating that the landfill cover system had lost its anti-seepage characteristics.

The hydraulic conductivity of compacted soil was closely related to the pores and cracks in the specimens. The hydraulic conductivity had nearly linear relationship with the ratio of surface cracks. The hydraulic conductivity increased with the increase of pore volume. This trend was especially obvious at the beginning of the wetting–drying cycles, then become unclear, and finally zeroed out, suggesting that the damage of soil structure mainly happened at the beginning of the wetting–drying cycles.

Water seepage

The development of water seepage in soil during the wetting–drying cycles is shown in Figs. 14 and 15. The closer the soils are to the wetting–drying boundary, the more obvious are the changes in the moisture content. With the increase in the burying depth, there were much less changes in moisture content in response to wetting–drying cycles. From Fig. 14, it can be seen that during the first three cycles, for the specimen with higher degree of compaction ($\rho = 1.65$ g/cm^3, $W_3 = 21$ %), the soil moisture content of 5 cm under its surface was nearly unchanged. In the fourth wetting–drying cycle, the soil moisture content at a depth of 5 cm was found to be influenced by the rainfall infiltration and evaporation, and increased from 20.5 to 21.5 %. Moreover, in the following 5 days of
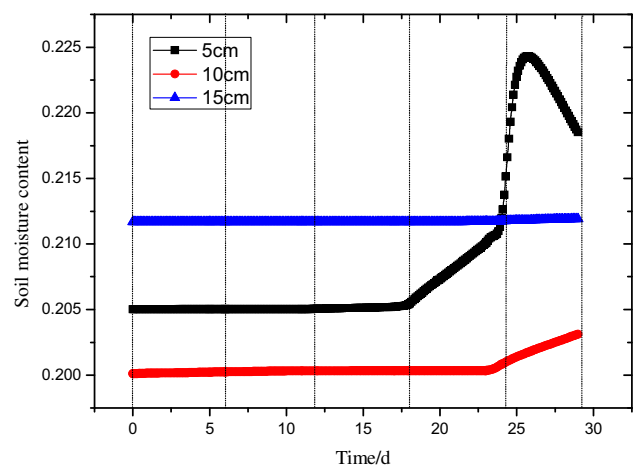

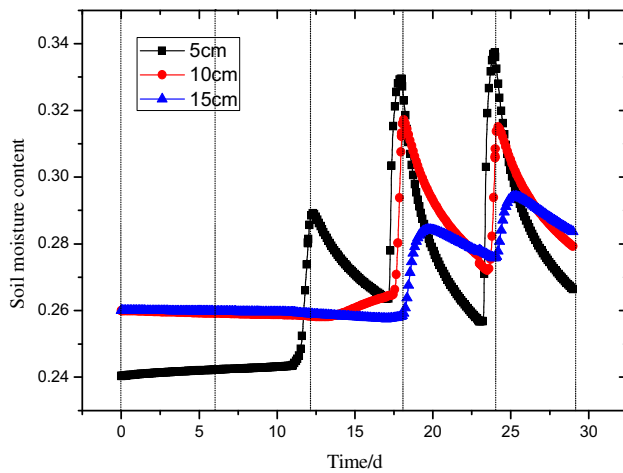Fig. 14 The water seepage of compacted loess ($\rho = 1.65$ g/cm^3, $W_3 = 21$ %) under wetting–drying cycles

Fig. 15 The water seepage of compacted loess ($\rho = 1.65$ g/cm^3, $W_5 = 25$ %) under wetting–drying cycles

drying, the soil moisture content first increased to 22.4 % and then decreased to 21.9 %. For the soils at a depth of 10 cm, the moisture content also increased in the fourth cycle and ultimately reached 20.3 %. For the soils at a depth of 15 cm, the moisture content nearly remained unchanged. All of the situations above indicated that in the fourth wetting–drying cycle, the cracks reopened and extended to a depth deeper than 5 cm. It seemed that the compacted soil layer at a depth of 10 cm had low permeability for anti-seepage.

Figure 15 shows that the moisture content of soil, which had lower density, was significantly influenced by the wetting–drying cycles. At the depth of 5 cm, the soil moisture content in the second cycle rapidly increased from 24.2 to 28.9 %. It gradually declined to 26.3 % after the 5 days of drying before the third cycle. Then in the following 1 day of wetting, the soil moisture content increased to 33.1 %. However, in the fourth cycle, the soil moisture content was found to first decline and then increase, which ultimately reached 33.8 %. In the last 5 days of drying, the moisture content decreased to 26.7 %. At the depth of 10 cm, the soil moisture content tended to increase and finally ended up at 27.9 % in the third cycle. At the depth of 15 cm, this increasing trend of moisture content did not appear until the fourth cycle. Moreover, in the second cycle, the cracks reached a depth of 5 cm under the surface. In the third cycle, the cracks reached a depth of 10 cm under the surface. Finally, in the fourth cycle, the cracks reached a depth of 15 cm under the surface. When the cracks reached the depth of 15 cm under the soil, the compacted soil had lost its anti-seepage capability and the rainfall could rapidly penetrate through the cracks.

Conclusions

In order to determine the anti-seepage capacity of Xiashu loess used as landfill cover system, the surface cracks, pores, hydraulic conductivity, and water seepage of the loess were systematically investigated in laboratory, respectively. The following conclusions can be made:

1. The CIF of the compacted soil samples rapidly increased with the number of wetting–drying cycles. But the increase in the CIF slowed down and gradually stabilized after three wetting–drying cycles. After four cycles, the CIF of the soil specimen ($\rho = 1.65$ g/cm^3, $W_5 = 25$ %) reached a maximum value of 0.15, indicating it cracked in the worst way. The minimum CIF of the soil specimen ($\rho = 1.65$ g/cm^3, $W_3 = 21$ %) was only 0.06.

2. In the loess, meso-pores were dominant and micro-pores were minor. As the number of wetting–drying cycles increased, the pore volume of soil was increased, but maximum pore size was nearly unchanged. After several wetting–drying cycles, the average diameter and proportion of macro-pores were also increased. However, those of the meso-pores were slightly decreased, and the diameter and the proportion of micro-pores nearly remained unchanged.

3. The wetting–drying cycles have significant influences on the hydraulic conductivity of compacted soils. After four wetting–drying cycles, the hydraulic conductivity of compacted soil increases about three orders of magnitude (from 8.3×10^{-7} to 1.5×10^{-5} cm/s), compared with the un-cracked soil. The hydraulic conductivity increased linearly with the increase of the amount of cracks. Moreover, the hydraulic conductivity firstly increased with the increase of pore volume, and then it gradually reached a stable level. The compactness of compacted soils had significant influence on the anti-seepage characteristics of the landfill cover system. After the action of wetting–drying cycles for nearly 1 month, the specimen ($\rho = 1.65$ g/cm^3, $W_5 = 25$ %) with relatively low compactness had cracks which had reached a depth of 15 cm under the soil surface. However, the cracks of compacted soils with high compactness only reached a depth of 5 cm.

4. It is recommended that the degree of compaction for compacted soils be strictly controlled to prevent leakage. The soils should be compacted at slightly higher than the optimum moisture content in order to reduce the likelihood of desiccation cracking occurrences due to the wetting–drying cycles.

References

Albrecht BA, Benson CH (2001) Effect of desiccation on compacted natural clays. ASCE J Geotech Geoenviron 127(1):67–75

Basnett C, Bruner R (1993) Clay desiccation of a single-composite liner system. In: Geosynthetics'93 conference vancouver. 1329–1334

CJJ 17 (2004) Technical code for municipal solid waste sanitary landfill. China Architecture and Building Press, Beijing **(in Chinese)**

Döll P (1997) Desiccation of mineral liners below landfills with heat generation. ASCE J Geotech Geoenviron 123(11):1001–1009

Egloffstein TA (2001) Natural bentonites-influence of the ion exchange and partial desiccation on permeability and self-healing capacity of bentonites used in GCLs. Geotext Geomembr 19:427–444

Hewitt PJ, Philip LK (1999) Problem of clay desiccation in composite lining systems. Eng Geol 53:107–113

Klein R, Baumann T, Kahapka E, Niessner R (2001) Temperature development in a modern municipal solid waste incineration (MSWI) bottom ash landfill with regard to sustainable waste management. J Hazard Mater B 83:265–280

Lecocq N, Vandewalle N (2003) Dynamics of crack opening in a one-dimensional desiccation experiment. Phys A 321:431–441

Li JH, Zhang LM (2011) Study of desiccation crack initiation and development at ground surface. Eng Geol 123(4):347–358

Li JH, Zhang LM, Li X (2011) SWCC and permeability function for unsaturated cracked soil. Can Geotech J 48(7):1010–1031

Miller CJ, Mi H, Yesiller N (1998) Experimental analysis of desiccation crack propagation in clay liners. J Am Water Resour Assoc 34(3):677–686

Montes HG, Duplay J, Martinez L, Escoffier S, Rousset D (2004) Structural modifications of Callovo–Oxfordian argillite under hydration/dehydration conditions. Appl Clay Sci 25:187–194

Montes-H G, Duplay J, Martinez L, Geraud Y, Rousset-Tournie B (2003) Influence of interlayer cations on the water sorption and swelling–shrinkage of MX80 bentonite. Appl Clay Sci 23:309–321

Rayhani MHT, Yanful EK, Fakher A (2008) Physical modeling of desiccation cracking in plastic soils. Eng Geol 97:25–31

Tang C, Shi B, Liu C, Zhao L, Wang B (2008) Influencing factors of geometrical structure of surface shrinkage cracks in clayey soils. Eng Geol 101:204–217

Tang C, Cui Y, Tang A, Shi B (2010) Experiment evidence on the temperature dependence of desiccation cracking behavior of clayey soils. Eng Geol 141(3–4):261–266

Xue Q, Lu H, Li Z, Liu L (2014a) Cracking, water permeability and deformation of compacted clay liners improved by straw fiber. Eng Geol 178:82–90

Xue Q, Lu H, Li Z, Zhao Y, Liu L (2014b) The metal ions release and microstructure of coal gangue corroded by acid-based chemical solution. Environ Earth Sci 71:3235–3244

Yesiller N, Miller CJ, Inci G, Yaldo K (2000) Desiccation and cracking behavior of three compacted landfill liner soils. Eng Geol 57:105–121

Zhou Y, Rowe RK (2003) Development of a technique for modelling clay liner desiccation. Int J Numer Anal Met 27:473–493